Microchimica Acta (2018) 185: 496
https://doi.org/10.1007/s00604-018-3035-8

ORIGINAL PAPER

Colorimetric determination of dopamine by exploiting the enhanced oxidase mimicking activity of hierarchical $NiCo_2S_4$-rGO composites

Yanying Wang[1] · Li Yang[1] · Yaqin Liu[1] · Qingbiao Zhao[2] · Fang Ding[3] · Ping Zou[1] · Hanbing Rao[1] · Xianxiang Wang[1]

Received: 9 July 2018 / Accepted: 28 September 2018 / Published online: 4 October 2018

Abstract

A composite consisting of $NiCo_2S_4$ and reduced graphene oxide (rGO) was prepared via a hydrothermal process. Compared to individual $NiCo_2S_4$ nanomaterials or reduced graphene oxide, the composite exhibits enhanced oxidase-like activity. It is found that dopamine (DA) inhibits the ability of $NiCo_2S_4$-rGO to oxidize the substrate 3,3′,5′,5′-tetramethylbenzidine (TMB) to form blue colored ox-TMB. Based on these findings, a colorimetric method for determination of DA was worked out. The absorption, best measured at 652 nm, increases linearly in the 0.5–100 μM DA concentration range, and the limit of detection is 0.42 μM. This method was successfully applied to the detection of DA in spiked human serum samples.

Keywords Hybrid nanostructure · Oxidase mimetic · Synergistic effect · Colorimetric assay · Human serum sample

Introduction

Dopamine supports human sensing capability and physical activity, but abnormal level of dopamine often lead to agitation, addiction and diseases such as Parkinsonism, acquired immune deficiency syndrome (AIDS), senile dementia and schizophrenia [3–5]. A variety of physicochemical methods have been developed to detect dopamine, including field effect transistor (FET)-based biosensor [6], fluorometry [7–10], chromatography [11, 12], electroanalysis [13–16] and capillary electrophoresis [17]. These methods are of high precision and good reproducibility, but not easy to be observed by bare eyes. Colorimetry possesses several advantages, such as convenience, low cost and visual detection. However, natural enzymes can be easily influenced by environmental changes, which restricts their practical application. Much attention has been paid to the research of artificial enzyme with higher stability in the application in colorimetric detection. It was reported that bovine serum albumin (BSA) stabilized Au clusters have high intrinsic peroxidase-like activity, and a simple, high sensitive and selective method was developed for xanthine detection in harsh chemical environment [18]. A novel approach has been proposed to sensitively and selectively detect hydrogen peroxide based on a bimetallic (Co/2Fe) metal-organic framework with dual enzyme mimetic activity [19]. In addition, a colorimetric sensing of dopamine based on high oxidase-mimic activity of Fe/NC-800 hybrid was developed [20]. These works demonstrated that mimic enzymes have great potential in biomedical analysis and environmental monitoring.

The substrate recognition and catalytic function of enzymes are essentially determined by their supramolecular

The authors wish it to be known that, in their opinions, Yanying Wang, Li Yang and Yaqin Liu should be regarded as joint First Authors.

Electronic supplementary material The online version of this article (https://doi.org/10.1007/s00604-018-3035-8) contains supplementary material, which is available to authorized users.

✉ Hanbing Rao
rhb@sicau.edu.cn

✉ Xianxiang Wang
xianxiangwang@hotmail.com

[1] College of Science, Sichuan Agricultural University, Xin Kang Road, Yucheng District, Ya'an 625014, People's Republic of China

[2] Nanshan District Key Lab for Biopolymers and Safety Evaluation, Shenzhen Key Laboratory of Polymer Science and Technology, Guangdong Research Center for Interfacial Engineering of Functional Materials, College of Materials Science and Engineering, Shenzhen University, Shenzhen 518060, People's Republic of China

[3] Key Laboratory of Polar Materials and Devices, Ministry of Education, Department of Electronic Engineering, East China Normal University, Shanghai 200241, People's Republic of China

structure [21]. Particularly, it has been found that graphene is effective for anchoring active metal catalysts [22]. To mimic the special supramolecular structure, nano-sized hierarchical architecture of $NiCo_2S_4$ on reduced graphene oxide was synthesized through hydrothermal process. Several nanomaterials have been applied for colorimetric analysis with good response to dopamine detection [23–26]. We synthesized hierarchical $NiCo_2S_4$-rGO nanocomposites and evaluated the nanocomposite materials as an oxidase mimic, and the substrate TMB was transformed into oxidized TMB. The hierarchical $NiCo_2S_4$-rGO nanocomposites exhibit an enhanced oxidase-like activity compared to the individual components, demonstrating the synergistic catalytic effect between $NiCo_2S_4$ and reduced graphene oxide. The presence of dopamine causes a blue color fading of $NiCo_2S_4$-rGO-TMB system. Based on these results, a colorimetric method was developed to determine dopamine in human serum samples. This is the first report to use $NiCo_2S_4$-rGO nanocomposite as an oxidase mimic to detect dopamine.

Experiment and methods

Chemicals and reagents

Graphite, sulfuric acid (H_2SO_4), phosphorus pentoxide (P_2O_5), potassium persulfate ($K_2S_2O_8$), potassium permanganate($KMnO_4$), $Co(NO_3)_2{\cdot}6H_2O$, $Ni(NO_3)_2{\cdot}6H_2O$, ethanol, $Na_2S{\cdot}9H_2O$, hexamethylenetetramine, o-phenylenediamine (OPD), 3,3′,5,5′-tetramethylbenzidine (TMB), t-Butanol (TBA), p-benzoquinone (PBQ), superoxide dismutase (SOD), dopamine and dimethyl sulfoxide (DMSO) were purchased from Macklin Co Ltd. (Shanghai, China, http://www.macklin.cn/). Histidine, phenylalanine, L-cysteine,glutathione,ascorbic acid,bovine serum albumin,uric acid,glucose, glycine, tyrosine and lysine were purchased from Aladdin Chemistry Co. Ltd. (Shanghai, China, http://aladdin.company.lookchem.cn/). All chemical reagents used are analytical reagent grade without further treatment, and ultrapure water was used throughout the study.

Preparation of graphene oxide

To prepare graphene oxide, it is necessary to oxidize commercial graphite power. Specifically, graphite (3 g) and concentrated H_2SO_4 (12 mL) were heated to 80 °C, then P_2O_5 (2.5 g) and $K_2S_2O_8$ (2.5 g) were added. The reaction liquid was cooled down naturally after stirring for 2 h, followed by dilution with 500 mL deionized water and kept overnight in ambient atmosphere. The final peroxidation product was obtained after centrifugation and natural drying. 15 g $KMnO_4$ was gradually added into 120 mL H_2SO_4 and kept below 20 °C. Then the temperature of the suspension was set as 35 °C for another 2 h after stirring for 2 h. The mixture was transferred into ice bath under vigorous stirring, and 700 mL deionized water was added dropwise until no obvious smoke was generated. Subsequently 20 mL H_2O_2 was added, resulting in bright yellow color of the mixture. The final product was washed with deionized water and HCl (10%) for serval times.

Fabrication of $NiCo_2S_4$-rGO composites

$Co(NO_3)_2{\cdot}6H_2O$ and $Ni(NO_3)_2{\cdot}6H_2O$ were added in proportion to aqueous ethanol, then hexamethylenetetramine was added. The mixture was stirred for 30 min, and a transparent pink solution was obtained. The mixture was then transferred into an autoclave, kept at 80 °C for 10 h, cooled to room temperature and washed for several times with deionized water. The obtained precursor was naturally dried. Next, the Ni-Co precursor was added into ultrasound-treated GO suspension. Then 0.5 g of $Na_2S{\cdot}9H_2O$ was added under stirring. The dark brown solution was kept at 160 °C for 8 h, centrifuged, and washed for several times. The final product was vacuum-dried at 40 °C. Bare $NiCo_2S_4$ was prepared in similar way in the absence of GO.

Oxidase mimic activity and steady-state kinetic studies

The hierarchical $NiCo_2S_4$-rGO nanocomposites catalytically oxidize TMB and cause a color of blue, resulting in the characteristic absorption band at 652 nm. First of all, 60 μL TMB (30 mM in dimethyl sulfoxide, DMSO) was added into 895 μL acetate buffer (pH = 4.0). Subsequently, 45 μL hierarchical $NiCo_2S_4$-rGO suspension (1 $mg{\cdot}mL^{-1}$) was added into the analysis system. After the end of incubation for 35 min at 25 °C, the absorbance of the analysis system at 652 nm was measured with UV–Vis spectroscopy. To evaluate the kinetic of $NiCo_2S_4$-rGO composite, 60 μL TMB with various concentrations, 45 μL $NiCo_2S_4$-rGO (1 $mg{\cdot}mL^{-1}$) and 895 μL acetate buffer were added, and the absorbance of the mixed reaction solution at 652 nm within 25 min were recorded. The kinetic parameters were calculated by Michaelis-Menten equation:

$$v = V_{max} \times [S]/K_m + [S],$$

in which [S] refers to the substrate concentration, V_{max} and K_m refers to the maximal reaction velocity and the Michael is constant, respectively.

Colorimetric detection of dopamine

To accurately investigate the capability of the $NiCo_2S_4$-rGO nanocomposite for determination of dopamine, 45 μL of

catalyst suspension and equivalent amount of TMB were added into acetate buffer (pH = 4.0). Then, various concentrations of dopamine were introduced into the mixture to reach a total volume of 3 ml. The changes in the absorbance at 652 nm were recorded by UV–Vis spectrometry. The dopamine concentration was determined by a calibration plot of the absorbance ($\Delta A = A_0$-A) at 652 nm, where A refers to the absorbance of dopamine sample of different concentrations and A_0 refers to the absorbance of the blank samples. For the real sample analysis, human serum samples from two donors were obtained with written informed consent (The project was approved by the hospital of Sichuan Agricultural University).

Characterization

The morphologies of $NiCo_2S_4$-rGO nanostructures were characterized by transmission electron microscope (TEM, JSM4800F, JEOL, Japan) and scanning electron microscope (SEM, JEOL2100F, JEOL, Japan). To analyze the crystalline structure, elemental composition and pore structure were analyzed by using X-ray diffractometer (XRD, DX-2700, Dan Dong, China). The chemical composition of the $NiCo_2S_4$-rGO composite was examined with X-ray photoelectron spectrometer (XPS, ESCALAB 250Xi, Boyue, China). UV-Vis spectrophotometer (Beijing Purkinje General Instrument Co. Ltd., Beijing, China) was used to record the absorption spectra and evaluate the oxidase-like activity of the material.

Results and discussion

Choice of materials

Generally, in order to increase the sensitivity of metal sulfide nanoparticles, composites of these metal sulfide nanoparticles with other materials can be synthesized. Graphene and its derivatives such as graphene oxide, possess large surface-to-volume ratio and high chemical stability. These advantages have contributed to the detection of biological macromolecules [27, 28]. It would be of great interest to explore them in multicomponent systems for synergistic properties. Graphene oxide was chosen to reduce the chances for particles agglomeration and resulted in maximum enzymatic activity of $NiCo_2S_4$ for colorimetric detection. The composite materials enhance the fast electron transfer involved during redox process [29]. In comparison, the method described by Chen et al. has low detection limit [20], but the detection of our method covering a wider range. It was reported that silver-based nanozymes (peroxidase-like) hybrid with other metals (Au, Pt, and Pd) were explored for monitoring ascorbic acid concentration [30]. For comparison, the synthesis processing of our method has the advantages of easily available raw materials and high cost-effectiveness. Moreover, the hydrothermal method used in this study is inexpensive, feasible and not easy to be contaminated.

Characterization of the anocomposite

As shown in Scheme 1, $NiCo_2S_4$-rGO composite was synthesized by a two-step approach. Firstly, under the precipitation of hexamethylenetetramine, with the increase of pH value of the reaction solution, Ni-Co precursor were formed from a reaction of Co^{2+} and Ni^{2+} cations. In order to form the hierarchical structure, Ni-Co precursor was added into ultrasound-treated GO solution under whisking and then the mixture was transferred into an autoclave for reaction. In hydrothermal processing, the hydrophilic Ni-Co precursor was sulfonated to form $NiCo_2S_4$ through an anion-exchange reaction under the attraction of the functional groups on the GO surface [31]. With the reduction of oxygenated functional groups, the GO turned into rGO.

The interconnected $NiCo_2S_4$ particles exhibits a flower-like morphology formed by stacked nanosheets (Fig. 1a). The thickness of these particles ranges from hundreds of nanometers to several micrometers as shown in Fig. 1b. The surface of $NiCo_2S_4$ appears to be much coarser compared to the Ni-Co precursor, mainly due to the rapid ion exchange and the Kodak effect in the process of vulcanization [32]. The TEM image further confirms the rough surface (Fig. 1c). As expected, $NiCo_2S_4$-rGO composite showed a layered porous structure composed of rumpled rGO nanoscale (Fig. 1d, e). Results shown that there were flower-like structures, while the reduced graphene oxide limited the stacking process of $NiCo_2S_4$ nanosheets (Fig. S1). This architecture can provide enough active sites for oxidation reduction. By comparing with Fig. 1c, the TEM image of $NiCo_2S_4$-rGO shown in Fig. 1f shows that the crumpled rGO nanosheets wrap around $NiCo_2S_4$ nanomaterials.

XRD patterns (Fig. S2a) shows that the peaks for all the samples can be indexed to (220), (311), (400), (511), and (440) plane reflections of the $NiCo_2S_4$ (JCPDS no. 43–1477). Lattice stripes are caused by the following crystal planes including 0.54 nm (111), 0.33 nm (220) and 0.28 nm (311), which are similar to the XRD pattern we obtained, and proves the presence of $NiCo_2S_4$ in $NiCo_2S_4$-rGO composite. Because of the low temperature of the reaction, the Ni-Co precursor has poor crystallinity. The Ni-Co precursor can be matched to $Ni_{0.75}Co_{0.25}(CO_3)_{0.125}(OH)_2 \cdot 0.38H_2O$ (JCPDS No.40–0216), as shown in Fig. S3. In general, rGO peak should be located at around 23.5°, the cracks can be due to the collapse of some crystal surfaces. The EDS spectrum further proves the presence of Co, Ni, S and C in the $NiCo_2S_4$-rGO composite (Fig. S2b). It should be noted that the signals of Pt and Cl in the EDS spectrum are attributed to the instrument itself. The above results indicate that $NiCo_2S_4$ has been successfully attached onto the surface of rGO nanosheets.

The analysis of X-ray photoelectron spectroscopy (XPS) is detailed in the Electronic Supporting Material (ESM).

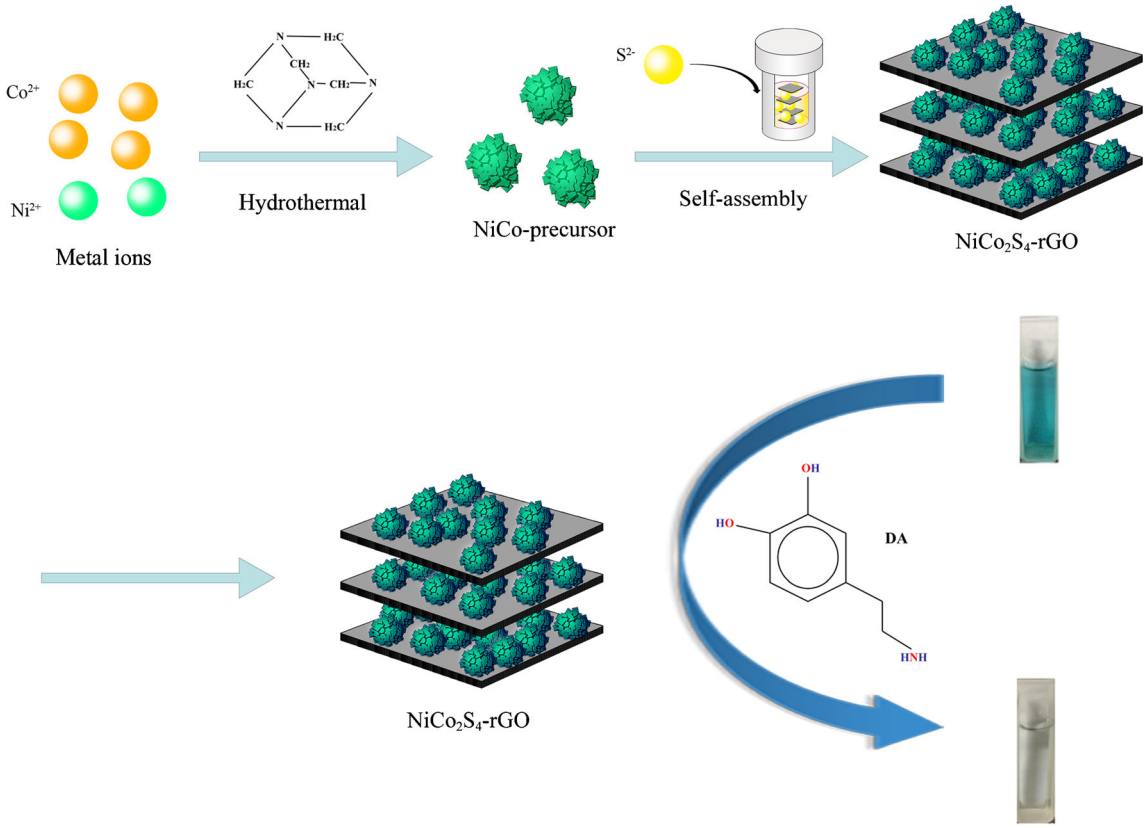

Scheme 1 Schematic diagram of the fabrication procedure for $NiCo_2S_4$-rGO composites and the colorimetric assay

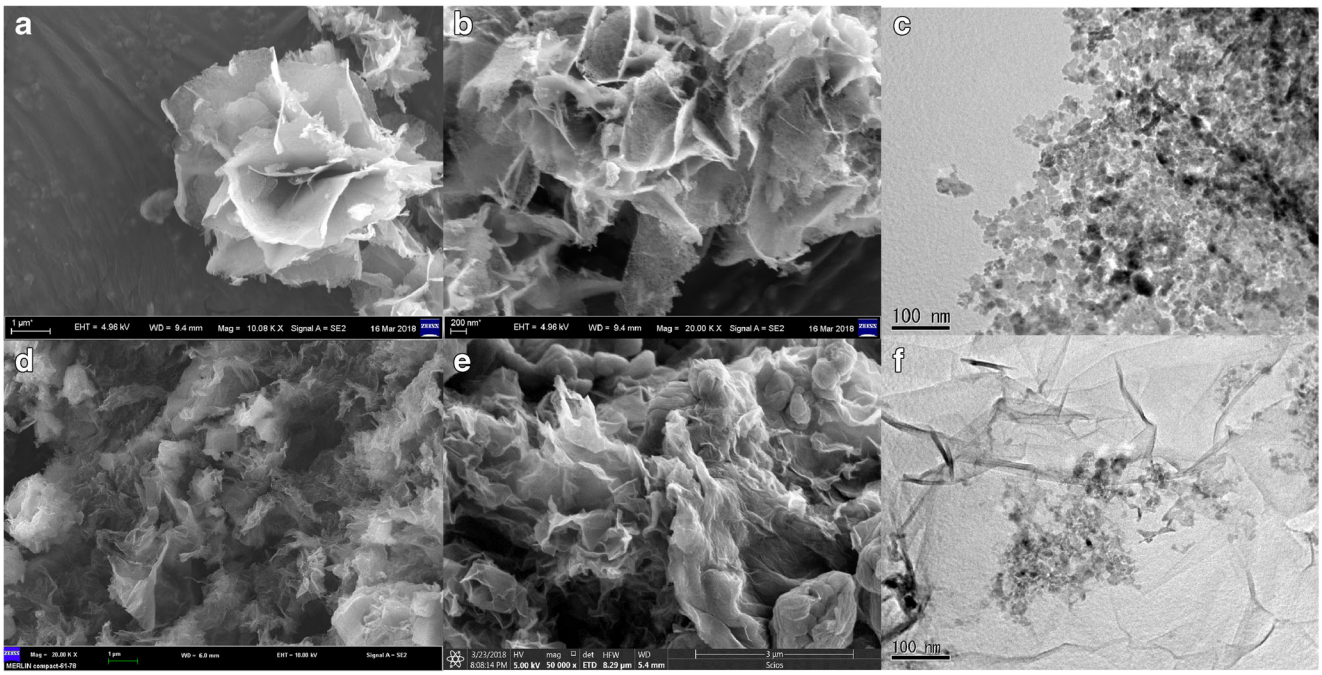

Fig. 1 **a, b** SEM and **c** TEM images of the $NiCo_2S_4$; **d, e** SEM and **f** TEM images of the $NiCo_2S_4$-rGO

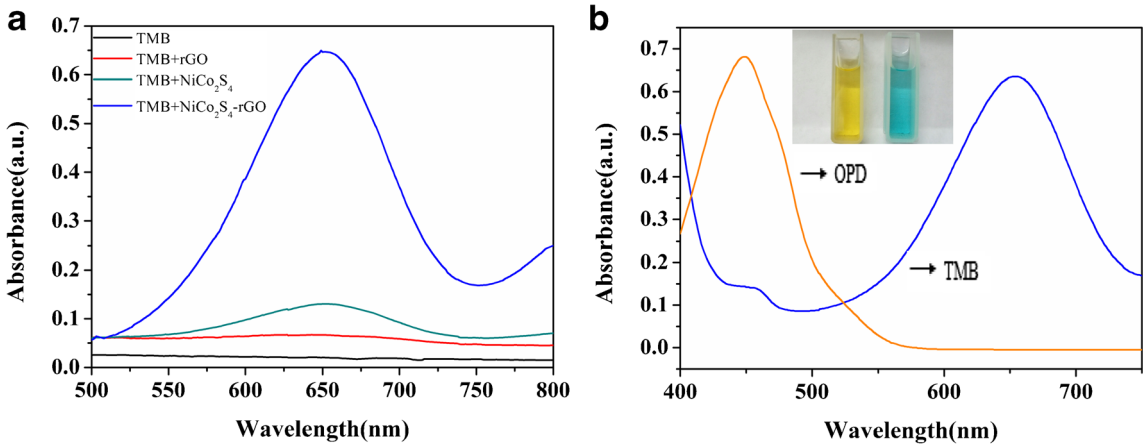

Fig. 2 **a** UV-Vis absorption spectra and visual color changes of TMB, TMB + rGO, TMB + $NiCo_2S_4$-rGO, TMB+ $NiCo_2S_4$, respectively. Conditions: pH 4.0 acetate buffer, TMB 0.6 mM, catalyst 1 mg·mL^{-1}, 25 °C for 35 min incubation. **b** $NiCo_2S_4$-rGO composite material catalyzing the oxidation of various substrates to produce different colors

Oxidase-like activity and steady-state kinetic of $NiCo_2S_4$-rGO

TMB was used as the substrate to evaluate the catalytic performance of $NiCo_2S_4$-rGO. The activity of oxidase-activity of the rGO, single $NiCo_2S_4$ were compared with $NiCo_2S_4$-rGO nanocomposite. As shown in Fig. 2a, rGO and single $NiCo_2S_4$ show weak catalytic activity for TMB oxidation. $NiCo_2S_4$-rGO nanocomposite exhibited good catalytic activity, and the increase of catalytic activity can be attributed to the hierarchical porous structure of $NiCo_2S_4$ nanometer and the larger specific surface area of rGO. The significant improvement on catalytic performance of $NiCo_2S_4$-rGO is attributed to the synergistic effect of $NiCo_2S_4$ and rGO.

To further confirm the oxidase-like catalytic activity of $NiCo_2S_4$-rGO composite, the oxidation reactions of two typical oxidase substrates of TMB and OPD were investigated, showing blue and light yellow in the process of oxidation. Their oxidized products have the maximum absorbance peaks at 652 and 450 nm, respectively (Fig. 2b). These phenomena prove that the intrinsic oxidase-like property of $NiCo_2S_4$-rGO composite. The dependency of the catalytic activity of the $NiCo_2S_4$-rGO composite material on TMB concentration and interaction time were also studied (Fig. S5a-b). The catalytic activity of $NiCo_2S_4$-rGO was evaluated under different temperatures. As shown in Fig. S5c, $NiCo_2S_4$-rGO showed higher oxidase activity in a wide temperature range, particularly near room temperature. It has been reported that the catalytic activity of rGO/Cu_8S_5/PPy depends largely on pH value, for determination of H_2O_2 and phenol [33]. The influence of pH values on $NiCo_2S_4$-rGO was evaluated. The data of Fig. S5d show that the catalytic activity of $NiCo_2S_4$-rGO was dependent on pH, and the absorbance reaches the maximum value at pH = 4. Accordingly, pH and temperature was set as 4.0 and 25 °C, respectively, as the optimum conditions. Moreover, over 90% of the catalytic capability of the $NiCo_2S_4$-rGO is still retained even after 20 days (Fig. S6), indicating good stability.

In order to study the oxidase activity of $NiCo_2S_4$-rGO, TMB was used as a single variable for steady-state kinetic analysis under the mechanism of Michaelis-Menten kinetics (Fig. S7). By applying the molar attenuation coefficient of 39,000 M^{-1} cm^{-1}, the absorbance value was converted to the blue product concentrations. According to the Michaelis-

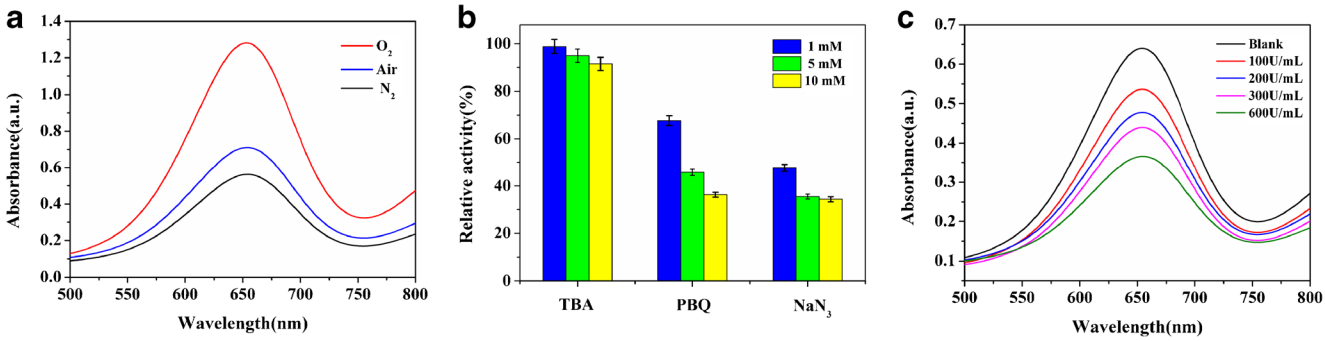

Fig. 3 **a** UV-Vis spectrum of $NiCo_2S_4$-rGO-TMB system in N_2/O_2 saturated system under optimal conditions. **b** Inhibition of different scavenger for $NiCo_2S_4$-rGO-TMB system. **c** Effect of SOD with different concentration for $NiCo_2S_4$-rGO-TMB system. Reaction conditions: 0.6 mM TMB; 45 μg·L^{-1} $NiCo_2S_4$-rGO; 15 min reaction time; pH 4.0; room temperature

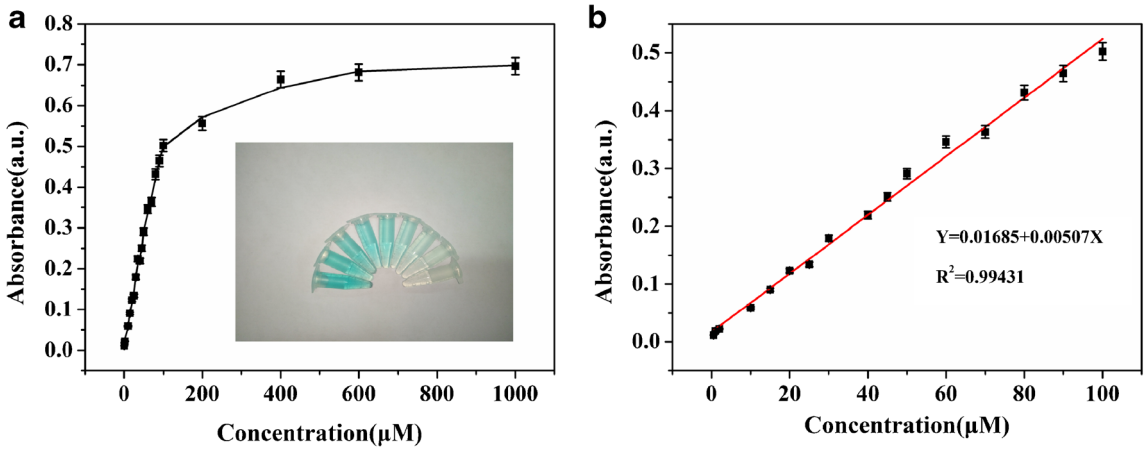

Fig. 4 **a** Absorbance changes of TMB solutions at 652 nm with different contents of dopamine according to the left-hand graph **b** The photograph exhibits the corresponding calibration line in the range of 0.5–100 μM

Menten equation: $1/v = (K_m/V_{max})\ (1/[S]) + 1/V_{max}$, the Michaelis constant (K_m) represents the intensity of intermolecular binding affinity, thus the K_m value was calculated with the Line-weaver-Burk dual reciprocal graph. The results are summarized in Table S1.

Possible mechanism of oxidase-like activity

To find out the possible mechanism of oxidase-like activity of $NiCo_2S_4$-rGO, the O_2-dependent catalytic oxidation experiment of TMB was performed. As shown in Fig. 3a, the catalytic activity increased significantly under O_2-saturaed condition. However, the catalytic activity of $NiCo_2S_4$-rGO was inhibited under N_2-staturated condition, indicating the importance of dissolved oxygen in the reaction system. The catalytic mechanism of this mimic nano-oxidase may be due to the capability for activation of O_2 to generate reactive oxygen species (ROS) in the TMB oxidation reaction [34]. As shown in Fig. 3b, the presence of TBA had no obvious effect on the reaction, indicating a few of •OH was produced. SOD, PBQ were used to scavenge superoxide radicals ($O_2^{\bullet-}$), and NaN_3 was selected to trap singlet molecular oxygen atoms ($^1O_2$). After adding these scavengers, the absorbance intensity significantly decreased (Fig. 3b, c). The results indicate generation of $^1O_2$ and $O_2^{\bullet-}$ in the catalytic process. In a word, with $NiCo_2S_4$-rGO acting as catalysts to activate oxygen molecules, generating reactive oxygen intermediates ($^1O_2$ and $O_2^{\bullet-}$). The produced ROS trap the electrons supplied by substrates, and then oxidized the substrates [35, 36]. During the entire process, the function of $NiCo_2S_4$-rGO composites is similar to that of oxidases.

Performance of $NiCo_2S_4$-rGO oxidase mimic for dopamine *detection*

The presence of dopamine inhibits oxidase activity of $NiCo_2S_4$-rGO nano-enzyme, resulting in discoloration and decreased absorbance. Based on the $NiCo_2S_4$-rGO, a reliable and low cost colorimetric method was developed for dopamine detection. Clearly, the absorbance increases with the increase of dopamine concentration (Fig. 4a). It shows good linear relationship in the range of 0.5–100 μM, and the linear

Table 1 Comparison with previous reports on the detection of dopamine

Materials	Catalytic property	LOD (μM)	Linearity range (μM)	Ref.
AuNRs	Colorimetric assay	0.03	0.1–10,000	[37]
AuNPs	Colorimetric assay	0.094	0–1	[38]
Protein-templated Fe_2O_3 microspheres	Electrochemical sensor	0.03	0.2–115	[39]
HNP-PtTi alloy/GCE	Electrochemical sensor	3.2	4–500	[40]
Silica-coated CdTe QDs	Fluorometric	0.0125	0.05–30	[41]
MoS_2 QDs	Fluorometric	0.01	0.1–100	[42]
Fe/NC-800	Oxidase mimics	0.01	0.01–40	[20]
$CuFe_2O_4/Cu_9S_8$/PPy	Peroxidase mimics	1.0	2–20	[24]
CuS-rGO	Peroxidase mimics	0.47	2–100	[25]
$NiCo_2S_4$-rGO composite	Oxidase mimics	0.42	0.5–100	This work

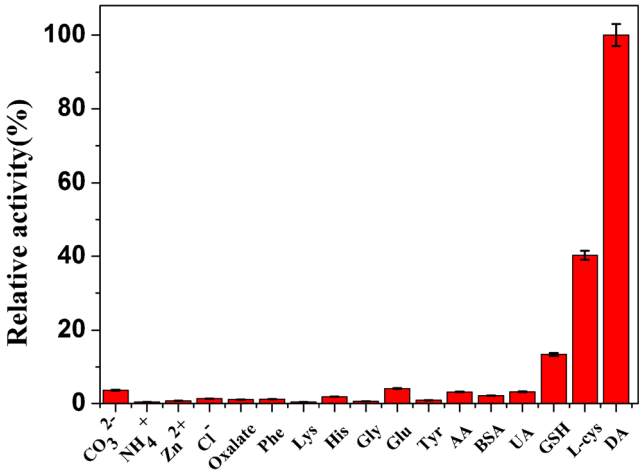

Fig. 5 Relative absorbance changes of 300 μM CO_3^{2-}, NH_4^+, Zn^{2+}, Cl^-, oxalate, Phe, Lys, His, Gly, Glu, Tyr; 30 μM of dopamine, UA; 3 μM AA, GSH, L-cys; 1 mg·mL^{-1} BSA

regression equation can be expressed as $\Delta A = 0.01685 + 0.00507\ C_{dopamine}$ ($R^2 = 0.99431$, $n = 16$), as shown in Fig. 4b. The detection limit is as low as 0.42 μM, which was calculated through the equation $LOD = 3S_0/K$, where S_0 means the standard deviation of blank measurements and K represents the slope of calibration line. Compared with other reported approaches (Table 1), the present method demonstrates high sensitivity for dopamine detection.

Selectivity

To determine the effects of interfering substances on dopamine detection in human serum, selectivity analyses were performed. The typical interferents, including CO_3^{2-}, NH_4^+, Zn^{2+}, Cl^-, oxalate, phenylalanine (Phe), L-histidine (His), lysine (Lys) glycine (Gly), glucose (Glu), L-tyrosine (Tyr), L-cysteine (L-cys), bovine serum albumin (BSA), uric acid (UA), ascorbic acid (AA) and glutathione (GSH) were tested. As shown in Fig. 5, these compounds did not cause significant color changes except for GSH and L-cys. In practical analysis, the interference of biothiols can be resolved by N-ethylmaleimide as the masking reagent for thiols [43]. Overall, the system shows good selectivity in the determination of dopamine.

Detection of dopamine in real samples

Human serum samples were used to evaluate the determination of dopamine. The samples (5 mL) were obtained from the hospital, and the coagulant was added rapidly. These serum samples were pretreated by high speed refrigerated centrifuge. Then the supernatant was separated and stored and stored at 4 °C. It should be noted that in order to ensure the dopamine concentrations were in the linear range and reduce the effects of interference, the serum samples were diluted with ultrapure water. The calibration plot was obtained by spiking the serum samples with standard dopamine solution. The absorbance changes of the serum samples at 652 nm was recorded, then the diluted concentration of dopamine was calculated by calibration plot. In order to evaluate the accuracy of the method, standards of dopamine in various amounts were added in diluted human serum samples, and recoveries were calculated. The recoveries in human serum sample were in the range of 102.9 and 107.9% (Table 2). Thus, this method is reliable for the analysis of complex biological samples.

Conclusion

In conclusion, $NiCo_2S_4$ nanomaterials on porous reduced graphene oxide sheets were synthesized by a hydrothermal method. The $NiCo_2S_4$-rGO nanocomposites were used as an oxidase mimic system to detect dopamine. The hierarchical $NiCo_2S_4$-rGO nanocomposites exhibited superior oxidase-like activity compared to individual $NiCo_2S_4$ nanomaterials and rGO nanosheets, indicating a synergistic effect among the components in the composites. In addition, dopamine can significantly inhibit the oxidase-like activity of the $NiCo_2S_4$-rGO composite. Based on these results, a reliable and low-cost colorimetric detection method for quantitative determination of dopamine is proposed. However, the catalytic activity of this material needs to be further improved. It is not suitable for detecting substances with strong reducibility in human serum. In order to avoid excessive effects on colorimetric detection, the pretreatment of samples is typically required. Overall, this study presents the fabrication of a new type of oxidase-like nanozyme

Table 2 Results for the determination of dopamine concentration in diluted human serum samples. ($n = 3$, 95% confidence level)

Sample	Spiking concentration (μM)	Determined concentration (μM)	RSD (%)	Recovery (%)
	5	5.15 ± 0.43	3.4	102.9
Serum 1	10	10.66 ± 1.22	4.6	106.6
	20	20.74 ± 1.13	2.2	103.7
	5	5.28 ± 0.29	1.7	105.7
Serum 2	10	10.76 ± 0.40	1.5	107.6
	20	21.58 ± 1.07	2.0	107.9

and provides a reliable colorimetric method for dopamine detection in human serum samples.

Acknowledgments This work was supported by a grant from the National Natural Science Foundation of China (21305097) and the 2016 undergraduate innovation training program of Sichuan Agricultural University (04054674).

Compliance with ethical standards The author(s) declare that they have no competing interests.

References

1. Chiu C, Moss CF (2007) The role of the external ear in vertical sound localization in the free flying bat, *Eptesicus fuscus*. J Acoust Soc Am 121(4):2227–2235
2. Leaf-nosed bat, in: Encyclopædia Britannica, Encyclopædia Britannica Online, 2009
3. Castro SL, Zigmond MJ (2001) Stress-induced increase in extracellular dopamine in striatum: role of glutamatergic action via N-methyl-D-aspartate receptors in substantia nigra. Brain Res 901(1–2):47–54
4. Vonk J, Shackelford TK (2012) The Oxford handbook of comparative evolutionary psychology. In: Nathan PE (ed) Oxford library of psychology. Oxford University Press, New York, p 574
5. Sajid M, Nazal MK, Mansha M, Alsharaa A, Jillani SMS, Basheer C (2016) Chemically modified electrodes for electrochemical detection of dopamine in the presence of uric acid and ascorbic acid: a review. Trends Anal Chem 76:15–29
6. Park SJ, Lee SH, Yang H, Park CS, Lee C-S, Kwon OS, Park TH, Jang J (2016) Human dopamine receptor-conjugated multidimensional conducting polymer nanofiber membrane for dopamine detection. Acs Appl Mater Inter 8(42):28897–28903
7. Shen J, Sun C, Wu X (2017) Silver nanoprisms-based Tb(III) fluorescence sensor for highly selective detection of dopamine. Talanta 165:369–376
8. Cheng Y, Wu J, Guo C, Li X-G, Ding B, Li Y (2017) A facile water-stable MOF-based "off-on" fluorescent switch for label-free detection of dopamine in biological fluid. J Mater Chem B 5(13):2524–2535
9. Xu B, Su Y, Li L, Liu R, Lv Y (2017) Thiol-functionalized single-layered MoS_2 nanosheet as a photoluminescence sensing platform via charge transfer for dopamine detection. Sensor Actuat B-Chem 246:380–388
10. Diaz-Diestra D, Thapa B, Beltran-Huarac J, Weiner BR, Morell G (2017) L-cysteine capped ZnS:Mn quantum dots for room-temperature detection of dopamine with high sensitivity and selectivity. Biosens Bioelectron 87:693–700
11. Schumacher F, Chakraborty S, Kleuser B, Gulbins E, Schwerdtle T, Aschner M, Bornhorst J (2015) Highly sensitive isotope-dilution liquid-chromatography–electrospray ionization–tandem-mass spectrometry approach to study the drug-mediated modulation of dopamine and serotonin levels in Caenorhabditis elegans. Talanta 144:71–79
12. Cudjoe E, Pawliszyn J (2014) Optimization of solid phase microextraction coatings for liquid chromatography mass spectrometry determination of neurotransmitters. J Chromatogr A 1341:1–7
13. Wang H-H, Chen X-J, Li W-T, Zhou W-H, Guo X-C, Kang W-Y, Kou D-X, Zhou Z-J, Meng Y-N, Tian Q-W, Wu S-X (2018) ZnO nanotubes supported molecularly imprinted polymers arrays as sensing materials for electrochemical detection of dopamine. Talanta 176:573–581
14. Ping J, Wu J, Wang Y, Ying Y (2012) Simultaneous determination of ascorbic acid, dopamine and uric acid using high-performance screen-printed graphene electrode. Biosens Bioelectron 34(1):70–76
15. Mashhadizadeh MH, Yousefi T, Nozad Golikand A (2012) A nickel hexacyanoferrate and poly(1-naphthol) hybrid film modified electrode used in the selective electroanalysis of dopamine. Electrochim Acta 59:321–328
16. Li Y, Gu Y, Zheng B, Luo L, Li C, Yan X, Zhang T, Lu N, Zhang Z (2017) A novel electrochemical biomimetic sensor based on poly(cu-AMT) with reduced graphene oxide for ultrasensitive detection of dopamine. Talanta 162:80–89
17. Zhang L, Qv S, Wang Z, Cheng J (2003) Determination of dopamine in single rat pheochromocytoma cell by capillary electrophoresis with amperometric detection. Electrochim Acta 792(2):381–385
18. Wang X-X, Wu Q, Shan Z, Huang Q-M (2011) BSA-stabilized au clusters as peroxidase mimetics for use in xanthine detection. Biosens Bioelectron 26(8):3614–3619
19. Yang H, Yang R, Zhang P, Qin Y, Chen T, Ye F (2017) A bimetallic (co/2Fe) metal-organic framework with oxidase and peroxidase mimicking activity for colorimetric detection of hydrogen peroxide. Microchim Acta 184(12):4629–4635
20. Chen Q, Liang C, Zhang X, Huang Y (2018) High oxidase-mimic activity of Fe nanoparticles embedded in an N-rich porous carbon and their application for sensing of dopamine. Talanta 182:476–483
21. Hammes-Schiffer S, Benkovic SJ (2006) Relating protein motion to catalysis. Annu Rev Biochem 75(1):519–541
22. Xing M, Wang J (2016) Nanoscaled zero valent iron/graphene composite as an efficient adsorbent for co(II) removal from aqueous solution. J Colloid Interf Sci 474:119–128
23. Zhu Y, Yang Z, Chi M, Li M, Wang C, Lu X (2018) Synthesis of hierarchical Co_3O_4@NiO core-shell nanotubes with a synergistic catalytic activity for peroxidase mimicking and colorimetric detection of dopamine. Talanta 181:431–439
24. Yang Z, Ma F, Zhu Y, Chen S, Wang C, Lu X (2017) A facile synthesis of $CuFe_2O_4/Cu_9S_8$/PPy ternary nanotubes as peroxidase mimics for the sensitive colorimetric detection of H_2O_2 and dopamine. Dalton T 46(34):11171–11179
25. Dutta S, Ray C, Mallick S, Sarkar S, Sahoo R, Negishi Y, Pal T (2015) A gel-based approach to design hierarchical CuS decorated reduced graphene oxide nanosheets for enhanced peroxidase-like activity leading to colorimetric detection of dopamine. J Phys Chem C 119(41):23790–23800
26. Yang Z, Zhu Y, Chi M, Wang C, Wei Y, Lu X (2018) Fabrication of cobalt ferrite/cobalt sulfide hybrid nanotubes with enhanced peroxidase-like activity for colorimetric detection of dopamine. J Colloid Interf Sci 511:383–391
27. Wei H, Wang E (2013) Nanomaterials with enzyme-like characteristics (nanozymes): next-generation artificial enzymes. Chem Soc Rev 42(14):6060–6093
28. Qian J, Yang X, Yang Z, Zhu G, Mao H, Wang K (2015) Multiwalled carbon nanotube@reduced graphene oxide nanoribbon heterostructure: synthesis, intrinsic peroxidase-like catalytic activity, and its application in colorimetric biosensing. J Mater Chem B 3(8):1624–1632
29. Nasir M, Nawaz MH, Latif U, Yaqub M, Hayat A, Rahim A (2017) An overview on enzyme-mimicking nanomaterials for use in electrochemical and optical assays. Microchim Acta 184(2):323–342
30. He W, Wu X, Liu J, Hu X, Zhang K, Hou S, Zhou W, Xie S (2010) Design of AgM bimetallic alloy nanostructures (M = au, Pd, Pt) with tunable morphology and peroxidase-like activity. Chem Mater 22(9):2988–2994

31. Juan Y, Chang Y, Xiaoming F, Changtai Z, Jieshan Q (2015) Ultrafast self-assembly of graphene oxide-induced monolithic NiCo–carbonate hydroxide nanowire architectures with a superior volumetric capacitance for supercapacitors. Adv Funct Mater 25(14):2109–2116
32. Yang J, Duan X, Guo W, Li D, Zhang H, Zheng W (2014) Electrochemical performances investigation of NiS/rGO composite as electrode material for supercapacitors. Nano Energy 5:74–81
33. Yanzhou J, Yan G, Guangdi N, Maoqiang C, Zezhou Y, Ce W, Yen W, Xiaofeng L (2017) Synthesis of rGO/Cu_8S_5/PPy composite nanosheets with enhanced peroxidase-like activity for sensitive colorimetric detection of H_2O_2 and phenol. Part Part Syst Charact 34(3):1600233
34. He W, Liu Y, Yuan J, Yin J-J, Wu X, Hu X, Zhang K, Liu J, Chen C, Ji Y, Guo Y (2011) Au@Pt nanostructures as oxidase and peroxidase mimetics for use in immunoassays. Biomaterials 32(4):1139–1147
35. Shen X, Liu W, Gao X, Lu Z, Wu X, Gao X (2015) Mechanisms of oxidase and superoxide Dismutation-like activities of gold, silver, platinum, and palladium, and their alloys: a general way to the activation of molecular oxygen. J Am Chem Soc 137(50):15882–15891
36. Tao Y, Ju E, Ren J, Qu X (2015) Bifunctionalized mesoporous silica-supported gold nanoparticles: intrinsic oxidase and peroxidase catalytic activities for antibacterial applications. Adv Mater 27(6):1097–1104
37. Teo PS, Rameshkumar P, Pandikumar A, Jiang Z-T, Altarawneh M, Huang NM (2017) Colorimetric and visual dopamine assay based on the use of gold nanorods. Microchim Acta 184(10):4125–4132
38. Leng Y, Xie K, Ye L, Li G, Lu Z, He J (2015) Gold-nanoparticle-based colorimetric array for detection of dopamine in urine and serum. Talanta 139:89–95
39. Chen X, Liu Q, Liu M, Zhang X, Lin S, Chen Y, Zhuang J, Yang D-P (2018) Protein-templated Fe_2O_3 microspheres for highly sensitive amperometric detection of dopamine. Microchim Acta 185(7):340
40. Zhao D, Yu G, Tian K, Xu C (2016) A highly sensitive and stable electrochemical sensor for simultaneous detection towards ascorbic acid, dopamine, and uric acid based on the hierarchical nanoporous PtTi alloy. Biosens Bioelectron 82:119–126
41. Wang B, M-m C, H-q Z, Wen W, Zhang X-h, S-f W (2017) A simple and sensitive fluorometric dopamine assay based on silica-coated CdTe quantum dots. Microchim Acta 184(9):3189–3196
42. Liu X, Zhang W, Huang L, Hu N, Liu W, Liu Y, Li S, Yang C, Suo Y, Wang J (2018) Fluorometric determination of dopamine by using molybdenum disulfide quantum dots. Microchim Acta 185(4):234
43. Xue Q, Cao X, Zhang C, Xian Y (2018) Polydopamine nanodots are viable probes for fluorometric determination of the activity of alkaline phosphatase via the in situ regulation of a redox reaction triggered by the enzyme. Microchim Acta 185(4):231